Physics in Medicine & Biology

IPEM Institute of Physics and Engineering in Medicine

PAPER • OPEN ACCESS

Commissioning of a water calorimeter as a primary standard for absorbed dose to water in magnetic fields

To cite this article: Leon de Prez *et al* 2019 *Phys. Med. Biol.* **64** 035013

IOP Publishing Phys. Med. Biol. 64 (2019) 035013 (12pp) https://doi.org/10.1088/1361-6560/aaf975

Physics in Medicine & Biology

IPEM Institute of Physics and Engineering in Medicine

OPEN ACCESS

PAPER

Commissioning of a water calorimeter as a primary standard for absorbed dose to water in magnetic fields

Leon de Prez[1,2,3], Jacco de Pooter[1], Bartel Jansen[1], Simon Woodings[2], Jochem Wolthaus[2], Bram van Asselen[2], Theo van Soest[2], Jan Kok[2] and Bas Raaymakers[2]

[1] VSL—Dutch Metrology Institute, Delft, The Netherlands
[2] Department of Radiotherapy, University Medical Center Utrecht, Utrecht, The Netherlands
[3] Author to whom any correspondence should be addressed.

E-mail: ldprez@vsl.nl

RECEIVED
26 October 2018

REVISED
30 November 2018

ACCEPTED FOR PUBLICATION
13 December 2018

PUBLISHED
29 January 2019

Keywords: dosimetry, MRgRT, primary standard, magnetic field, MRI-linac, calorimetry

Abstract

MRI guided radiotherapy devices are currently in clinical use. Detector responses are affected by the magnetic field and need to be characterized in terms of absorbed dose to water, D_w, against primary standards under these conditions. The aim of this study was to commission a water calorimeter, accepted as the Dutch national standard for D_w in MV photons and to validate its claimed standard uncertainty of 0.37% in the 7 MV photon beam of a pre-clinical MRI-linac in a 1.5 T magnetic field.

To evaluate the primary standard on a fundamental basis, realisation of D_w at 1.5 T was evaluated parameter by parameter. A thermodynamic description was given to demonstrate potential temperature effects due to the magneto-caloric effect (MCE). Methods were developed for measurement of depth, variation in detector distance and beam output in the bore of the MRI-linac. This resulted in D_w measurements with a magnetic field of 1.5 T and, after ramp-down, without magnetic field.

It was shown that the measurement of ΔT_w and calorimeter corrections are either independent of or can be determined in a magnetic field. The chemical heat defect, h, was considered zero within its stated uncertainty, as for 0 T. Evaluation of the MCE and measurements done during magnet ramp-down, indicated no changes in the specific heat capacity of water. However, variations of the applied monitor system increased the uncertainty on beam output normalization.

This study confirmed that the uncertainty for measurement of D_w with a water calorimeter in a 1.5 T magnetic field is estimated to be the same as under conventional reference conditions. The VSL water calorimeter can be applied as a primary standard for D_w in magnetic fields and is currently the only primary standard operable in a magnetic field that provides direct access to the international traceability framework.

1. Introduction

Several integrated MRI guided radiotherapy treatment devices are under development or in clinical use (Fallone 2014, Keall *et al* 2014, Lagendijk *et al* 2014, Mutic and Dempsey 2014). Dosimetry in the presence of a magnetic field, B, is not trivial because the energy deposition changes the secondary electrons trajectories that are influenced by the Lorentz force. Dose distributions change e.g. in build-up and penumbra regions, in the central beam region and at material or tissue interfaces (Raaijmakers *et al* 2008, Raaymakers *et al* 2004, Oborn *et al* 2010, Woodings *et al* 2018). The magnitude of these dose effects depends on the magnetic field strength and its orientation relative to the photon beam, material differences and density inhomogeneities. Not only the dose distribution is affected but also the response of commonly used dosimeters in terms of their calibration coefficient as e.g. described by van Asselen *et al* (2018). Traditionally, photon beams in radiotherapy are calibrated by collecting charge inside the air cavity of an ion chamber (see e.g. Andreo *et al* (2000), Aalbers *et al* (2008) and McEwen *et al* (2014)). Ion chamber response is affected by the magnetic field and depends on the magnetic field direction and the direction of the photon beam in relation to the orientation of the ion chamber (Meijsing *et al* 2009, Reynolds *et al* 2013,

Smit *et al* 2013). The quantity of absorbed-dose-to-water, D_w, in the unit J kg^{-1} (Seltzer *et al* 2011), is defined as 'the mean energy imparted, $d\bar{\varepsilon}$ by ionizing radiation to water of mass dm':

$$D_w = \frac{d\bar{\varepsilon}}{dm}. \quad (1)$$

Where the energy imparted, $d\bar{\varepsilon}$, is the sum of all energy deposits in the volume of mass dm. As photons do not have electrical charge and the interaction coefficients of photons and electrons with matter is unaffected by the magnetic field (Szymanowski *et al* 2015) only the electron fluence is affected by the magnetic field. The definition of the D_w in equation (1) therefore only depends on the total energy imparted by radiation and is suited to define the quantity of absorbed dose also in the presence of a magnetic field.

The goal in reference dosimetry is to determine D_w at a reference point in a homogeneous water phantom. This D_w value is subsequently used as a starting point for accelerator calibration and commissioning, usually by means of ion chambers. The most fundamental and direct method to calibrate ion chambers for reference dosimetry in terms of D_w in a magnetic field is against a primary standard[3] which is modified and characterized for application in a magnetic field. Alternatively, a detector is needed with a response that is not affected by the magnetic field or can be characterized accordingly, so it can be calibrated without magnetic field and used to calibrate ion chambers in a magnetic field. However, methods applying these detectors also need to be validated against a primary standard. This emphasises the need of a primary standard for ionizing radiation in the presence of magnetic fields.

Methods used in primary D_w determination in high-energy photon beams, described e.g. by Andreo *et al* (2000) and Seuntjens and Duane (2009), are: (1) standards using ionization chambers, (2) standards using ferrous sulphate (Fricke) solution, (3) standards based on either graphite or water calorimetry. Water calorimetry is based on the underlying assumption that energy imparted by ionizing radiation per unit of mass ($d\bar{\varepsilon}/dm$) is transferred to specific heat (dq) and ultimately appears as a temperature rise of water, dT_w, which leads to the fundamental relation:

$$D_w = dq = c_p \cdot dT_w \quad (2)$$

with c_p the specific heat capacity of water. If the assumption of complete energy conversion from deposited dose to heat is fulfilled, or if any discrepancy is well understood and taken into account, the calorimeter can be considered as the most fundamental and absolute method of the available techniques for the measurement of D_w (Seuntjens and Duane 2009). In magnetic fields, material or density inhomogeneities near the reference point affect the electron fluence and are undesired (O'Brien and Sawakuchi 2017). Therefore water calorimetry appears to be the most suitable primary measurement method for application in magnetic fields.

VSL developed a new water calorimeter as a primary standard for absorbed dose to water. It was designed and built for on-site measurements in photon beams of ^{60}Co, kV x-ray and MV photon beams, including MRI incorporated treatment machines (de Prez *et al* 2016a). The uncertainty for ^{60}Co and MV photon beams was established at 0.37% ($k = 1$). The agreement for D_w without magnetic field (i.e. at 0 T) and its uncertainty was international accepted by taking part in BIPM[4] key-comparisons (Büermann *et al* 2016, Picard *et al* 2017, Kessler *et al* 2018). The calorimeter has demonstrated its applicability on-site for conventional flattened and flattening filter free (FFF) high-energy photon beams (de Prez *et al* 2018). Based on the preliminary assessment of the calorimeter temperature sensors in a magnetic field, it was proposed that the uncertainty for MV photon beams at 1.5 T would not exceed that at a conventional 0 T field. Preliminary results were presented earlier (de Prez *et al* 2016b) and showed the feasibility of water calorimetry in the presence of a magnetic field.

The current study describes the characterization and commissioning of the VSL water calorimeter in the presence of a 1.5 T magnetic field of a 7 MV Elekta Unity MRI-linac. The aim of this study is to validate the claimed uncertainty of 0.37% ($k = 1$) for determination of absorbed dose to water in MV photon beams in the presence of a magnetic field.

2. Materials and methods

2.1. The wide bore hybrid MRI-linac system

The pre-clinical Elekta Unity hybrid MRI-linac system used in this study comprises a modified 1.5 T Philips wide bore MRI with 70 cm diameter and an Elekta 7 MV standing wave linear accelerator producing a flattening filter free (FFF) photon beam (Raaymakers *et al* 2009, Lagendijk *et al* 2014, Woodings *et al* 2018). The beam quality

[3] A primary standard is defined as a measurement standard obtaining a measurement result without relation to a measurement standard for a quantity of the same kind (OIML 2007).

[4] The Bureau Internationales des Poids et Mesures, BIPM in Sévres, is an international organization established by the Metre Convention, through which Member States act together on matters related to measurement science and measurement standards (www.bipm.org/).

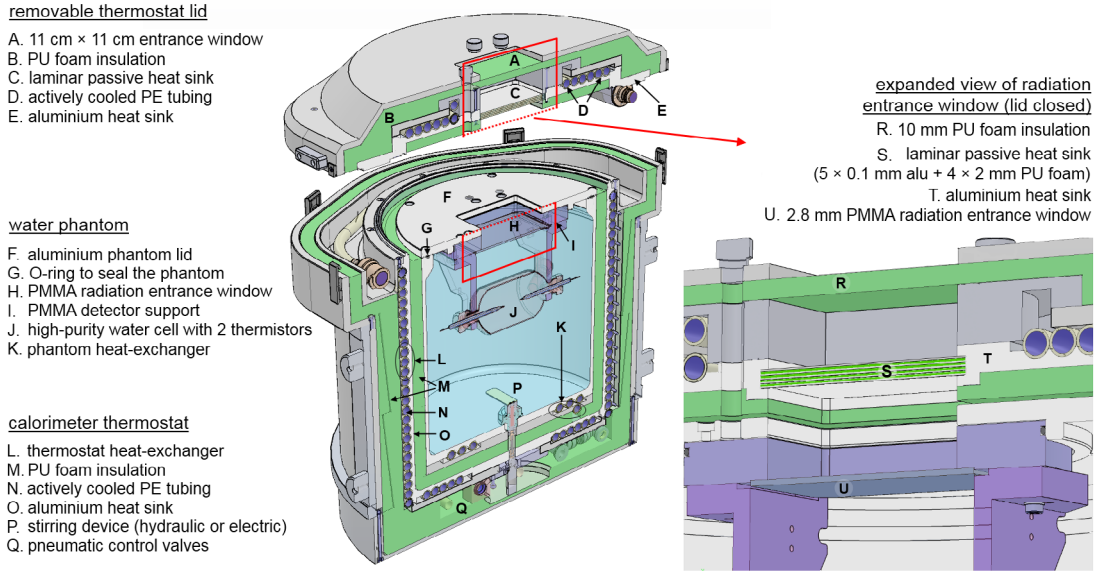

Figure 1. Cross-section of the calorimeter described in more detail by de Prez *et al* (2016a). It contains the high-purity cell at a measurement depth of 10 cm (left) and includes an expanded view of the radiation entrance window (right).

expressed in $TPR_{20,10}$ has a value of 0.701 and is, within its standard uncertainty independent of the presence of the magnetic field (van Asselen *et al* 2018). The accelerator is mounted on a ring 'inside' a low-field toroid to magnetically decouple it from the MRI (Overweg *et al* 2009). The ring allows for continuous rotation with an accelerator source to iso-centre distance of 143.5 cm. There is a beam-portal through the magnet and cryostat, however, the beam still passes through liquid helium and the cryostat wall. The described configuration provides for a transverse magnetic field relative to the beam. The linac is equipped with a multi-leaf collimator and an electronic portal imaging device (EPID) on the ring behind the beam exit side. A beam stopper is mounted behind the EPID. The MRI-linac is not equipped with conventional positioning tools such as alignment lasers, front pointer or a light field.

2.2. The VSL water calorimeter in the MRI-linac

The VSL calorimeter, shown in figure 1 and described elsewhere in detail (de Prez *et al* 2016a), is constructed of non-ferromagnetic materials for the purpose to be operated in a magnetic field. It contains a cylindrical water phantom operated at 4 °C to avoid convection due to temperature gradients. The beam enters the calorimeter at the centre of a removable lid through a square radiation window. A cylindrical high-purity water cell (HPC) made of thin-walled glass contains two negative temperature coefficient (NTC) thermal resistors, so called thermistors, glued at the tip of miniature glass pipettes. These are used to measure the radiation induced temperature change in water, ΔT_w. The thermistor probes are mounted 10 mm apart inside the HPC filled with argon-saturated ultra-pure water. Ion chambers can be calibrated directly inside the calorimeter water phantom. This is accomplished by using a detector mount that can accommodate either the calorimeter HPC or ion chambers on a replaceable detector mount.

Figure 2 shows the water calorimeter inside the 70 cm MRI-linac bore with the couch removed. It was mounted on an independent bridge with legs resting on the floor at both sides of the treatment machine (see figure 2(B)). The calorimeter was aligned in the centre of the beam using the EPID projection images providing a resolution of 0.2 mm at the point of measurement. The lateral position of the calorimeter was repeatedly verified using the EPID images at a gantry angle of 0°, i.e. with a vertical beam. Its SDD was determined to be 139.3 cm, i.e. 4.2 cm above iso-centre, using EPID images at a gantry angle of 90°. Changes in calorimeter height were checked regularly with two laser-distance meters (Leica Disto D810). These were positioned, with the laser beam in horizontal orientation, on a tripod outside the bore in low magnetic field (see figure 2(G)). The horizontal laser beams from the distance meters entering the bore were deflected downwards by 90° to measure the distance to the calorimeter reference plane and, with the calorimeter placed to the side, to the bottom of the bore (see figure 2(F)). The detector mount (figure 1(I)) was enabled also to rotate 90° remotely, i.e. without the need to access the water phantom. With this set-up the variation in SDD was measured with an uncertainty of 0.3 mm ($k = 1$), equivalent to better than 0.05% on the determination of D_w.

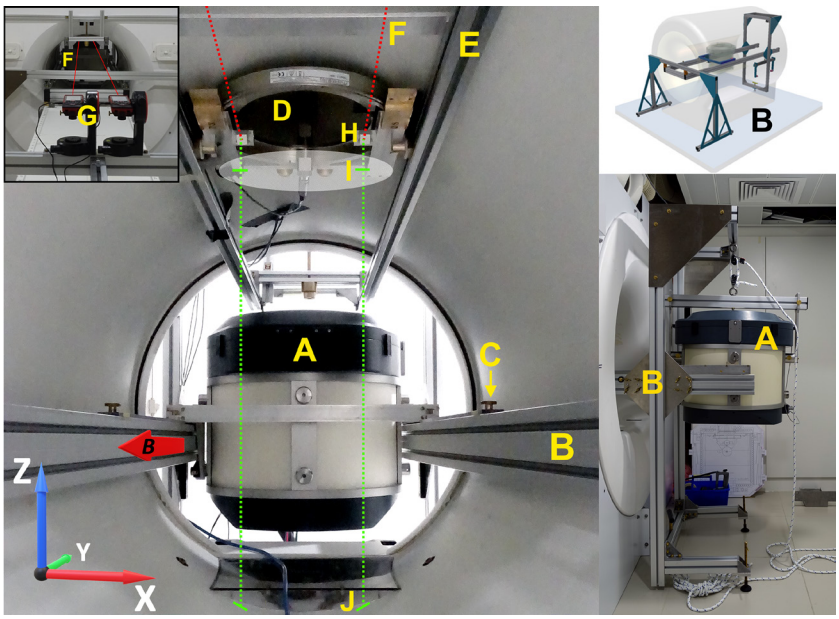

Figure 2. The water calorimeter phantom (A) positioned on two rails of a bridge (B), suspended outside the MRI-linac and fixed *Y* direction by two bolts on rulers (C) at both sides. An independent transmission monitor (D), fixed against the inside of the bore, on rails of a second bridge (E) served as the vertical reference point. Two laser-beams (F) from laser-distance meters outside the bore (G) are deflected in a right-angle downwards by 45° mirrors (H) to measure the vertical displacement of the calorimeter reference plane (I) in relation to the bottom of the bore (J).

2.3. Beam output monitoring

An external thin-window transmission monitor chamber (PTW 34014) was positioned in the MRI-linac bore, above the water calorimeter, as shown in figure 2(D). It was suspended from a second independent frame (figure 2(E)) that was not in direct mechanical contact with the frame of the calorimeter. In this study, no additional build-up material was placed on the entrance side of the transmission monitor to avoid any material inhomogeneities close to its sensitive volume. In an experiment prior to the calorimeter measurements this was found to be an improved method compared to the a monitor setup equipped with 2 mm additional build-up material. Sufficient electron build-up from the MRI cryostat wall was presumed to reach the monitor chamber in order to justify the removal of the additional 2 mm build-up material. The relative standard deviation of linac output at 1.5 T measured with the transmission monitor compared to a reference ion chamber inside a water phantom was 0.16% over a period of 4 d. The internal monitor of this particular pre-clinical MRI-linac was not used because it showed leaking behaviour based on instabilities that followed the ambient pressure.

2.4. Calorimetry in magnetic fields

The water calorimetric determination of absorbed dose, D_w, at the reference point in water, requires measurement of the radiation induced temperature change in water, ΔT_w, multiplied by the specific heat capacity of water, c_p (4207.5 J kg^{-1} K^{-1} at 4 °C) and several correction factors, correcting for chemical heat defects, h, undesired conductive heat flow, k_C, the presence of the calorimeter glass cell, k_{HPC} and geometrical deviations from reference conditions, k_R:

$$D_w = \Delta T_w \cdot c_p \cdot (1-h)^{-1} \cdot k_C \cdot k_{HPC} \cdot k_R. \quad (3)$$

Traditionally, the absorbed dose to water with calorimeters is determined without a magnetic field. Operation in a magnetic field requires understanding of the effect of the magnetic field on measured temperature change per unit of Gray. Any of the factors on the right-hand side of equation (3) could potentially be affected by the magnetic field. For commissioning and characterisation of the water calorimeter as a primary standard for D_w determination in the presence of magnetic fields, these factors are addressed in the following paragraphs and their relevance is described in relation to the presence or absence of a magnetic field.

2.4.1. Measurement of the water temperature change, ΔT_w

The radiation induced temperature change of water, ΔT_w, is measured by recording the resistance change of two thermistors, each connected to their own high-precision digital-multimeter (DMM). In a previous study the known magneto-resistance effect (MRE) on the resistance measurements was evaluated for two thermistor probes (de Prez *et al* 2016a). This was done between the poles of an electromagnet with the miniature glass pipettes containing thermistors, held perpendicular to the direction of the magnetic field ($\perp$). For a 1.5 T magnetic field

a resistance change, $\Delta R_{MR\perp}/R$, between −43 ppm and −24 ppm was observed for five temperatures between 0 °C and 23 °C. This was −38 ppm at 4.0 °C with a standard uncertainty of 4 ppm. For the measurement at 0 °C a melting-point of water was created by placing the thermistor probe in melting ice, an ice-point. This created a stable and constant temperature during half an hour in which the experiment took place and before the heat from the surroundings and the electromagnet melted the available ice. The variation of MRE over the measured range between the ice-point (at 0 °C) and room temperature was small, i.e. +19 ppm. Essential for the current study, however not reported earlier, was the inclusion of the ice-point, where the heat capacity of water (at the solid–liquid transition) is not defined. This showed agreement with the MRE in the liquid phase, above 0 °C. This confirmed that the thermistor resistance change in water at 4 °C was only caused by MRE and not by a change of the specific heat capacity of water, explained later.

The variation or MRE over the operational temperature range of the calorimeter (i.e. ~3.8 °C to ~4.2 °C) was shown to be negligible, resulting in negligible effect on the calorimetric measurement of ΔT_w.

However, measurement of the MRE with the probes in parallel direction between the electromagnet's poles was not possible due to the restricted space. To verify the effect of the magnetic field direction on ΔT_w, in the current study measurements were done in the bore of the MRI-linac with the thermistor probes both perpendicular ($\perp$) and in parallel ($\parallel$) direction to the magnetic field. The resistance change, $\left(R_{MR\parallel} - R_{MR\perp}\right)/R_{MR,\parallel}$, of the two thermistors was measured while rotating them by 90°.

2.4.2. *Water temperature effects in magnetic fields*

To understand the effect of the magnetic field, B, on the calorimetric determination of D_w and the actual water temperature, T_w, the subject is approached from the concept of entropy and the laws of thermodynamics. Franco *et al* (2018) gave an overview of the so-called magneto-caloric effect (MCE) in materials. This is also known as 'adiabatic demagnetization'. The MCE gives rise to an adiabatic temperature change due to the application or removal of an external magnetic field. It is defined as 'the reversible temperature change produced upon a magnetic field change in an adiabatic process'. It can be shown that the specific entropy, s, at constant pressure, p, can be expressed as a function of water temperature, T_w, and magnetic field, B, i.e. $s(T_w, B)$. It follows that:

$$\mathrm{d}s = \left(\frac{\delta s}{\delta T_w}\right)_{p,B} \mathrm{d}T_w + \left(\frac{\delta s}{\delta B}\right)_{p,T_w} \mathrm{d}B. \tag{4}$$

The 2nd law of thermodynamics defines entropy change, ds, for a reversible adiabatic process, such as the MCE, as:

$$\mathrm{d}s = \frac{\mathrm{d}q}{T_w}. \tag{5}$$

Where the specific heat flux, dq, is expressed in J kg^{-1}, and from equations (4) and (5) it follows that:

$$\mathrm{d}q = T_w \mathrm{d}s = T_w \cdot \left(\frac{\delta s}{\delta T_w}\right)_{p,B} \mathrm{d}T_w + T_w \cdot \left(\frac{\delta s}{\delta B}\right)_{p,T_w} \mathrm{d}B. \tag{6}$$

The specific heat capacity of water at constant pressure and constant magnetic field, $c_{p,B}$, is defined as $(\mathrm{d}q/\mathrm{d}T_w)_{p,B}$, $(=T_w \delta s/\delta T_w)$ thus, from this and equations (5) and (6) follows:

$$\mathrm{d}q = c_p \cdot \mathrm{d}T_w + T_w \cdot \left(\frac{\delta s}{\delta B}\right)_{p,T_w} \mathrm{d}B. \tag{7}$$

If the magnetic field is constant during a calorimeter measurement, with $\mathrm{d}B = 0$ T and $c_{p,B} = c_p$, then equation (7) is reduced to equation (2). This shows that with a constant magnetic field, B, a heat flux entering the system, the energy imparted by ionizing radiation causes a temperature change which only depends on the specific heat capacity of water. Variation of the magnetic field during calorimetry is therefore not recommended since this could give erroneous results in the measurement of D_w.

2.4.3. *Expected water temperature change due to the magneto-caloric effect*

Measurement of the water temperature, T_w, was done during magnet ramp-down from 1.5 T to 0 T to indicate any changes in c_p, if this would occur. The second term on the right of equation (7) is governed by the MCE. It shows that changing the magnetic field during calorimetry could lead to a change in water temperature that is not only the result of absorption of ionizing radiation but also of the MCE. Franco *et al* (2018) showed that on the application of a magnetic field strength, H (in A m^{-1}), under adiabatic conditions at temperature T_w, a temperature change $\mathrm{d}T_{w,ad,CE}/\mathrm{d}H$ is expected that is related to the vacuum permeability μ_0 ($4 \cdot \pi \cdot 10^{-7}$ N A^{-2}) and the specific magnetization per unit of temperature, $(\delta m/\delta T)_B$ in A m^2 kg^{-1} K^{-1}, at constant magnetic field strength, H:

$$\mathrm{d}T_{\mathrm{w,ad,MCE}} = -\frac{\mu_0 \cdot T_\mathrm{w}}{c_\mathrm{p}} \cdot \left(\frac{\delta m}{\delta T_\mathrm{w}}\right)_{\mathrm{p,H}} \mathrm{d}H. \tag{8}$$

With the magnetic field strength $H = B/(\mu_0(1+\chi_\mathrm{v}))$ and involving the dimensionless volume magnetic susceptibility, χ_v, this can be written as:

$$\mathrm{d}T_{\mathrm{w,ad,MCE}} = -\frac{T_\mathrm{w}}{(1+\chi_\mathrm{v}) \cdot c_\mathrm{p}} \cdot \left(\frac{\delta m}{\delta T_\mathrm{w}}\right)_{\mathrm{p,B}} \mathrm{d}B. \tag{9}$$

The specific magnetization, m, can be derived from the material's magnetization, M in A m^{-1}, which has a relation with the magnetic field strength and the volume magnetic susceptibility, χ_v:

$$m = \frac{M}{\rho} = \frac{\chi_\mathrm{v} \cdot H}{\rho} = \frac{\chi_\mathrm{v} \cdot B}{\rho \cdot \mu_0 \cdot (1+\chi_\mathrm{v})}. \tag{10}$$

The volume magnetic susceptibility for water is very small ($-9 \cdot 10^{-9}$). Therefore, at constant magnetic field, B, the specific magnetization at constant magnetic field, $(\delta m/\delta T)_\mathrm{B}$, can be expressed as:

$$\left(\frac{\delta m}{\delta T_\mathrm{w}}\right)_\mathrm{B} = \frac{B}{\rho \cdot \mu_0 \cdot (1+\chi_\mathrm{v})^2} \cdot \left(\frac{\delta \chi_\mathrm{v}}{\delta T_\mathrm{w}}\right)_\mathrm{B}. \tag{11}$$

Combining this with equation (9), the adiabatic temperature change due to the MCE can be obtained with:

$$\Delta T_{\mathrm{w,ad,MCE}} = -\int_{B_\mathrm{initial}}^{B_\mathrm{final}} \frac{T_\mathrm{w} \cdot B}{c_\mathrm{p} \cdot \mu_0 \cdot \rho \cdot (1+\chi_\mathrm{v})^2} \cdot \left(\frac{\delta \chi_\mathrm{v}}{\delta T_\mathrm{w}}\right)_\mathrm{B} \mathrm{d}B. \tag{12}$$

For diamagnetic materials, such as water, the temperature dependence of $(\delta\chi_\mathrm{v}/\delta T)_\mathrm{B}$ is small and constant over the range between 0 °C and 100 °C with a value of $[\delta\chi_\mathrm{v}/\delta T] = -1.1 \cdot 10^{-9}\,\mathrm{K}^{-1}$ (Rumble *et al* 2018). In this study, a calorimeter temperature drift was recorded during ramp-down of the MRI-magnet from 1.5 T to 0 T. If the heat capacity of water at 1.5 T is the same as at 0 T, this would result in an adiabatic temperature change of:

$$\Delta T_{\mathrm{w,ad,MCE}} = \frac{T_\mathrm{w} \cdot B^2}{2 \cdot c_\mathrm{p} \cdot \mu_0 \cdot \rho} \cdot \left[\frac{\delta \chi_\mathrm{v}}{\delta T_\mathrm{w}}\right] = -0.06\ \mu\mathrm{K}. \tag{13}$$

2.4.4. *The heat capacity of water in a magnetic field*

The coefficient that converts the measured radiation induced temperature change, ΔT_w, to the quantity of interest, D_w, is the specific heat capacity of water, c_p (4207.5 J kg^{-1} K^{-1} at 4 °C), obtained from literature at 0 T (IAPWS 2014). No substantial literature was found on c_p in magnetic fields or the effect of magnetic fields on c_p. With the MCE described above, equation (7) does not provide a value of c_p in a magnetic field. For this, c_p needs to be measured in a magnetic field, which is outside the scope of this study. However, to obtain an indication of a change in heat capacity between 0 T and 1.5 T, a calorimeter temperature measurement was performed during magnet ramp-down. A significantly larger change in water temperature than expected by the MCE, would then indicate a change of c_p.

2.4.5. *The chemical heat defect, h*

Situations for which full conversion of energy deposition into temperature rise is not fulfilled are indicated by the heat defect, h. For photon beams in water calorimetry the chemical heat effect is described by various authors, e.g. Domen (1982), Klassen and Ross (1997), Seuntjens and Palmans (1999) and Krauss and Kramer (2003) and summarized by Seuntjens and Duane (2009). The chemical heat defect in a water calorimeter is almost entirely caused by radiation-induced exo- or endothermic chemical reactions. VSL applies a sealed glass vessel (HPC) filled with a pure (hypoxic) water system which is saturated with Ar-gas to remove any remaining impurities. The VSL HPC is made of glass with Teflon™ seals in contact with the water. It undergoes a thorough cleaning process before it is filled. The preparation process, filling and Ar-saturation of the HPC has shown to be effective and reliable: i.e. with a successful fill no pre-irradiation is needed to reach a steady state zero heat-defect with $h = 0$ within the stated uncertainty of 0.2%. Linear energy transfer (LET) and dose-rate are known to influence the chemical heat defect. However, these properties of radiation do not fundamentally change for the MRI-linac used in this study compared to conventional linacs. It is unknown how the reaction constants for the chemical heat defect are affected. For the time being, it is assumed that also in the presence of a magnetic field, a zero-chemical heat defect is valid within the relative standard uncertainty of 0.2%.

2.4.6. *Correction for conductive heat flow, k_C*

The correction for conductive heat flow, k_C, is applied to correct for relative excess temperature rise, R_XS, due to non-water materials (HPC and probes, i.e. mainly glass) and dose distribution in the calorimeter water phantom

(Palmans 2000, Krauss 2006, de Prez *et al* 2016a). The dose distribution caused by a photon beam entering a water phantom changes with magnetic field strength. Potentially, k_C is also affected by the magnetic field induced changes in material thermal properties such as specific heat capacity, c_p, and heat conduction coefficient, k. However, this is not considered in the calculation of k_C. Seuntjens and Duane (2009) showed that the excess temperature effect, R_{XS}, is proportional to both c_p and k. Because $k_C = (1 - R_{XS})^{-1}$, any change in R_{XS} caused by a change in c_p or k has a second order effect on k_C. In the current literature no evidence could be found to indicate an effect on c_p or k caused by a magnetic field. k_C was determined with finite element simulation according to the heat transfer model described by de Prez *et al* (2016a). In this model only 1/4 of the beam and calorimeter were modelled with symmetry on the *XZ* and *YZ* planes (see figure 2). The model was based on conduction-only since the water density was maximal at 4 °C, avoiding density driven convection due to thermal gradients. The magnetic field dependence on the radiation induced excess heat of the HPC, was investigated by Monte Carlo calculations and shown to be smaller than 4%, affecting the overall k_C by less than 0.05%. Measured lateral and depth dose profiles were used as input for the heat transfer calculations. Since the applied model was based on a quarter geometry with symmetry on the *XZ* and *YZ*-planes, asymmetry of the MRI-linac beam profiles was accounted for by simulating only a profile shift in *X*-direction. The excess temperature, R_{XS}, was then calculated at reference points shifted in the opposite direction. Asymmetry of the crossline profile could not be simulated in a quarter geometry, however, the input crossline profile for the heat transport calculations were based on the mean $+X$ and $-X$ profiles to average the thermal effect approaching the ΔT_w measurement point from both sides. It must be noted that k_C does not account for beam radial non-uniformity. This is dealt with in correction factor k_R, shown in equation (3).

2.4.7. *Correction for perturbation of the glass cell, k_{HPC}*

The perturbation correction for the presence of the high-purity water cell and probes, k_{HPC} was measured in the MRI-linac both with and without 1.5 T magnetic field. For this purpose, a small ion chamber (PTW 31013) was placed in a water phantom. The ion chamber signal was measured repeatedly while it was inside the HPC and in water without HPC.

2.4.8. *Correction for geometrical deviations from reference conditions, k_R*

The correction, k_R, corrects for the deviation of the measurement conditions according to the defined reference geometry such as source detector distance (k_{SDD}), depth in water (k_d) and beam radial non-uniformity (k_{nu}):

$$k_R = k_{SDD} \cdot k_d \cdot k_{nu}. \tag{14}$$

In this study the reference SDD was 139.3 cm and the reference depth 10 g cm^{-2}. k_{SDD} and k_d are determined by applying respectively the inverse square law and photon beam effective attenuation, μ_{eff}, based on measured $TPR_{20,10}$ values, described by e.g. Andreo *et al* (2017). The calorimeter correction for beam radial non-uniformity, k_{nu}, at the position of the probe tips, 5 mm off-axis, was based on the measured crossline (X) and inline (Y) dose profiles and determined by the measured ratio at beam centre and 5 mm off-axis.

2.5. Calorimeter measurements

Measurements in the MRI-linac were performed in a 1.5 T magnetic field and, after ramp-down, repeated without magnetic field. Both measurement series, i.e. with and without magnetic field, were performed with the same high-purity cell, HPC, and thermistor probes (HPC #06 with thermistor probes serial numbers 13T023 and 15T006). Additionally, with and without magnetic field, the directional dependence of the HPC and probes was assessed. This was done by performing measurements with the HPC in parallel direction to the bore (and magnetic field) and in perpendicular direction. Variation in D_w measurements in the VSL ^{60}Co source before and after the measurements at UMCU were smaller than 0.05%, confirming chemically stable HPC and thermistor calibration during the measurements at UMCU. Pre-drifts and post-drifts were 120 s with intermediate heating drifts of 60 s at ~560 cGy min^{-1}. The nominal source surface distance (SSD) was set at 129.3 cm at a nominal depth of 10 g cm^{-2}, at the beam central axis. Deviations from nominal SDD and depth were measured according to the methods described earlier (de Prez *et al* 2016a) and corrected to nominal SSD and depth by applying k_R in equation (14). Within the two separate measurement series, i.e. with and without magnetic field, the readings were normalized to the transmission monitor inside the bore of the MRI-linac. These series cannot be directly compared since the response of transmission monitor was affected by the magnetic field.

3. Results

3.1. Magnetic field effects on the thermistor during HPC rotation

The HPC and probes were rotated in relation to the magnetic field to investigate the effect of the field direction on the calorimeter performance. Figure 3 shows the thermistor drift while rotating the HPC with thermistors from

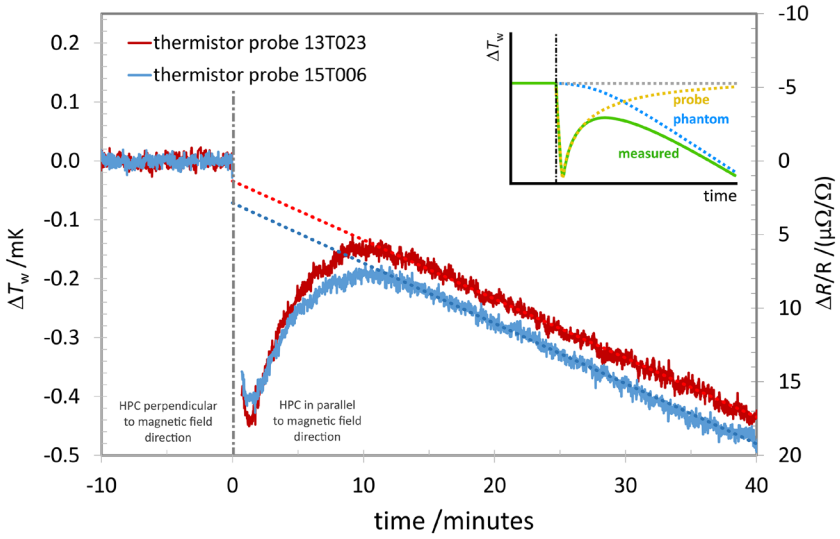

Figure 3. Calorimeter drift of two thermistors while rotating the HPC with thermistors from perpendicular to parallel direction in the magnetic field. The right-axis shows the actual relative resistance change, $\Delta R/R$, while the left-axis shows the equivalent in water temperature, ΔT_w, with a thermistor coefficient, α, of ~0.04 K^{-1}. The inset on the top-right corner illustrates the two presumed effects involved in a qualitative way: 'probe' cooling of the thermistor self-heat; 'phantom' movement of the phantom water.

perpendicular ($\perp$) to parallel ($\parallel$) direction. The first 40 s after rotation were discarded because of electrical noise due to movement of signal cables. Figure 3 shows that the rotation of the HPC causes a change in temperature drift. Presumably, this can be explained by two independent effects, illustrated by the inset on the top-right corner of the figure. The first effect (yellow line, marked 'probe') is caused by the movement of the water inside the HPC and causes an immediate drop of thermistor self-heat. Within about half an hour the self-heat is re-established to its initial conditions. The second effect (blue line, marked 'phantom') is caused by movement of the calorimeter phantom water outside the HPC. It causes a drop of water temperature outside the HPC resulting in a gradual temperature decrease at the position of the probes. A drop in phantom temperature is caused by a disturbance of the steady-state vertical temperature gradient in the phantom with relatively warm water at the top and colder water at the bottom. During steady-state, this gradient is intensified by a small influx of heat through the radiation entrance window (figure 1). The second effect leads to a slow background drift which usually takes days to re-establish the steady-state equilibrium. Within the time scale of the experiment, this effect can be approximated by a constant cooling drift. Both effects add up to the illustrated 'measured' temperature drift (green line, marked 'measured'). It is assumed that extrapolation of the linear part of the post-drift to time = 0 min coincides with the thermistor resistance just after rotation ($\parallel$). This results in resistance changes, $\Delta R_{MR,\perp}/R_{MR,\parallel}$ of +1.4 ppm and +2.9 ppm for respectively thermistors 13T023 and 15T006, which are smaller than the uncertainty of 4 ppm on the total thermistor MRE. An average value for the MRE of −38 ppm was obtained previously (de Prez *et al* 2016a) in a perpendicular orientation. Combining the values obtained in this study by correcting the probes MRE from $\perp$ to $\parallel$ leads to values for $\Delta R_{MR,\parallel}/R$ of respectively −36.6 ppm and −35.1 ppm for the current probes. The uncertainty on these values is estimated to remain 4 ppm.

3.2. Magnetic field effects on the calorimeter during ramp-down

The top of figure 4 shows the thermistor resistance change during magnet ramp-down from 1.5 T to 0 T with the probes in parallel direction to the magnetic field, $\Delta R_{MR\parallel}$. The drift was recorded from 3 h prior to 3 h after the start of the ramp down. The bottom of figure 4 shows the thermistor temperature drifts before the start (time $\leqslant$ 0 h) and after completion (time $\geqslant$ 0.5 h) of the ramp-down. The differences in temperatures between the two probes is smaller than 1.5 mK. This is within the uncertainty of the thermistors temperature calibration of 2 mK ($k = 2$). To obtain the temperature drifts, the thermistors resistances were corrected for the MRE determined in the previous paragraph. The difference in water temperature with and without magnetic field, T_w, is determined by extrapolation of the post-drift to the start of the ramp-down (time = 0 h). For thermistors 13T023 and 15T006 ΔT_w of respectively −0.16 mK and −0.13 mK was determined with an uncertainty of 0.20 mK ($k = 2$). The latter is based on an uncertainty of 4 ppm ($k = 1$) on the MRE and therefore ΔT_w does not deviate significantly from 0 K. The predicted temperature change due to adiabatic demagnetization, $\Delta T_{ad,MRE}$, of −0.06 μK, given by equation (13), is smaller than this uncertainty and therefore not detectable. Additionally, the bottom of figure 4 shows no change in slope of the temperature drift before and after ramp-down. This suggests that there were no changes in thermal properties of water such as heat conduction coefficient, used for the conductive heat flow correction, k_C. The non-detectable temperature change combined with the constancy of

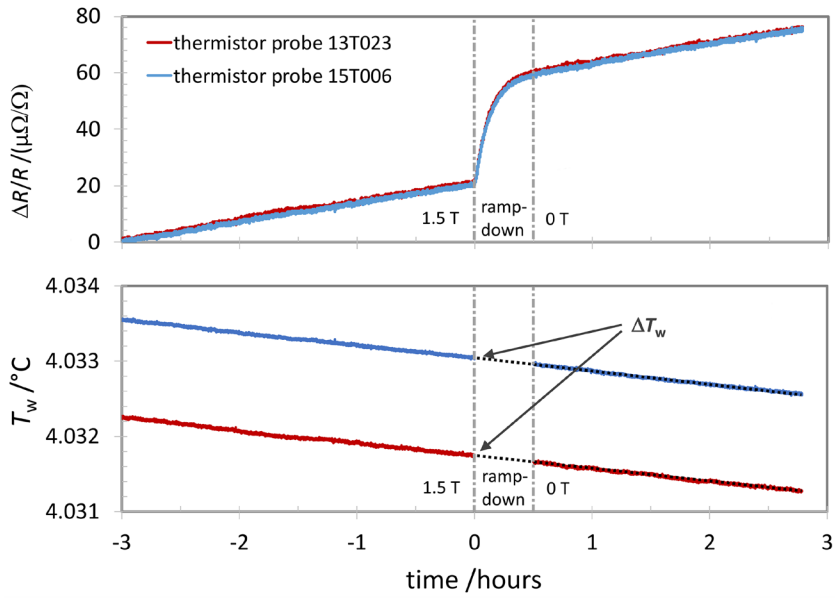

Figure 4. The thermistor resistance change, $\Delta R/R$ in ppm (top), and water temperature drift, T_w in °C (bottom), from 3 h before until 3 h after the start of the magnet ramp-down from 1.5 T to 0 T. The magnet ramp-down starts at time = 0 h.

temperature drift before and after ramp-down strongly suggests that there is no significant change in c_p between 0 T and 1.5 T. c_p is considered unchanged and no additional uncertainty was applied to c_p in a 1.5 T magnetic field.

3.3. Calorimeter correction factors

Table 1 shows the calculated correction factors for heat conduction, k_C, with and without magnetic field for both orientations of the calorimeter high-purity cell, HPC, perpendicular to the bore ($k_{C,\perp}$) and in parallel to the bore ($k_{C,\parallel}$). Differences are smaller than the assigned relative standard uncertainty for k_C calculation of 0.18% (de Prez *et al* 2016a).

The correction for the lateral position of the thermistor probes, k_{nu}, in equation (14) accounts for the position of the thermistor probes, nominally 5 mm off-axis. It is based on the position of the calorimeter, based on EPID images in the linac beam and on measured lateral profiles obtained from Woodings *et al* (2018) with an average dose shift of 2.4 mm in the *X*-direction, perpendicular to the bore. Because no internal markers were used for positioning of the calorimeter reference point, external structures were used. Therefore, and despite the 0.2 mm EPID resolution, the lateral positioning of the thermistors was estimated to be known within 1 mm. This corresponds to a type B relative standard uncertainty of 0.05% for the FFF beam of the MRI-linac, based on the dose gradients in the beam profiles. The radial non-uniformity correction at the position of the probes, corrected for lateral alignment of the calorimeter with the EPID images was between 1.0007 and 1.0025 with an average of 1.0014 and independent of magnetic field.

Table 1 also shows the measured corrections due to the perturbation and scatter of two high-purity glass cells (IDs #06 and #07) measured both with and without magnetic field. HPC #06 was used for the measurements described in this study. The measured values show that the respective correction factors with and without the presence of a magnetic field overlap within their assigned uncertainties. It can be concluded that the perturbation correction for the presence of the HPC is not affected by the magnetic field. Therefore, the assigned relative standard uncertainty is unchanged, i.e. 0.05% ($k = 1$).

Overall it can be concluded that calorimeter correction factors, k_C, k_{nu} and k_{HPC} can be determined by calculations or measurement but are not significantly affected by the presence of the magnetic field.

3.4. Calorimetry results parallel and perpendicular to the magnetic field

Calorimeter measurement parallel and perpendicular to the magnetic field are shown in figure 5. The right graph of figure 5 shows calorimetric D_w measurements in a 1.5 T magnetic field. Measurements were performed with the HPC in parallel and perpendicular direction to the magnetic field, resulting in average values for D_w normalized to the transmission monitor of respectively 0.6533 Gy/MU ($n = 77$) and 0.6544 Gy/MU ($n = 60$) both with a type A standard uncertainty of 0.05%. To compare the parallel and perpendicular values, the relative standard uncertainty was estimated to be 0.18%. This includes a 0.05% type B uncertainty on k_{nu} for positioning in the MRI-linac FFF beam and 0.16% for the day-to-day stability of the monitor ion chamber. The agreement

Table 1. Calculated correction factors for heat conduction, k_C and measured correction factors for perturbation of the calorimeter HPC both with and without magnetic field.

Correction	$B = 0$ T	$B = 1.5$ T
$k_{C,\perp}$	0.9976 (18)	0.9979 (18)
$k_{C,\parallel}$	0.9970 (18)	0.9969 (18)
$k_{nu,\perp}$	1.0013 (5)	1.0015 (5)
$k_{nu,\parallel}$	1.0014 (5)	1.0016 (5)
k_{HPC} (#06)	1.0033 (5)	1.0025 (5)
k_{HPC} (#07)	1.0031 (5)	1.0028 (5)

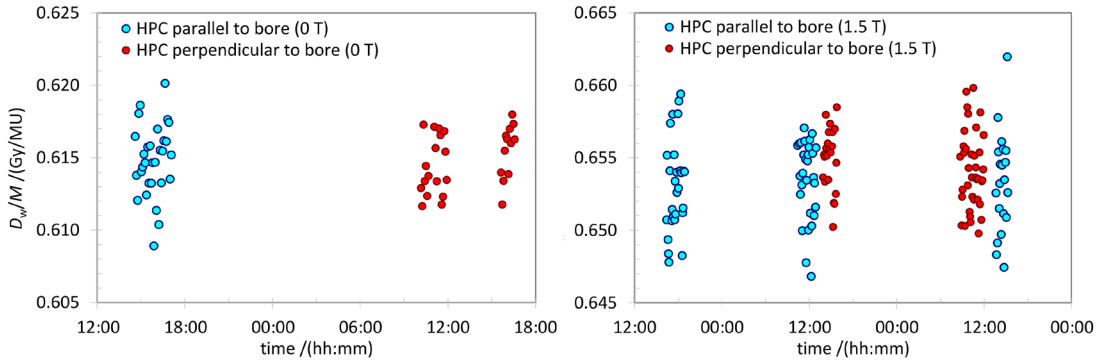

Figure 5. Corrected calorimetric D_w measurements in a 0 T magnetic field of an Elekta MRI-linac (left) and in the same machine with 1.5 T magnetic field (right). Both graphs show D_w measurements normalized to the transmission monitor in the bore with the HPC perpendicular and in parallel direction to the bore.

between the values obtained with the two HPC orientations was 0.17% and well within the expanded uncertainty 0.36% ($k = 2$).

The left graph of figure 5 shows D_w measurements performed with the HPC in parallel and perpendicular direction to the bore, at 0 T. This resulted in average values for D_w normalized to the transmission monitor of respectively 0.6148 Gy/MU ($n = 30$) and 0.6149 Gy/MU ($n = 29$) both with a type A standard uncertainty of 0.07%. In the same way as with the 1.5 T measurements, the relative standard uncertainty on these values was estimated to be 0.18%. The agreement between the values obtained with the two HPC orientations was 0.01, also well within the expanded uncertainty 0.36% ($k = 2$).

For both measurements at 1.5 T and at 0 T the differences between parallel and perpendicular orientation are within the estimated expanded uncertainties.

4. Discussion

The aim of this study was to characterize and commission for the first time the Dutch national standard for MV photon beams as a primary standard for absorbed dose to water, D_w, in magnetic fields and evaluate its previously claimed uncertainty of 0.37% ($k = 1$). Since a primary standard is defined as 'a measurement standard obtaining a measurement result without relation to a measurement standard for a quantity of the same kind' (OIML 2007), it cannot be compared to a more fundamental measurement standard. Agreement on an international level without magnetic field, e.g. organized by the BIPM (Allisy *et al* 2009), was shown by international comparisons (Picard *et al* 2017). However, due to the unique character of the VSL water calorimeter, comparison with equivalent standards in a magnetic field has not been possible. Therefore, a fundamental approach needed to be applied to commission the new primary standard in a magnetic field and evaluate its claimed uncertainty.

In the current study, the fundamental relation between radiation induced temperature change of the water, ΔT_w, and absorbed dose to water given by equation (3), was evaluated on a parameter by parameter basis. It was shown that the measurement of ΔT_w and most corrections, such as heat conduction, k_C, presence of non-water materials, k_{HPC}, and correction to reference geometry, k_R, in equation (3) are either independent of the magnetic field or can be determined in the presence of a magnetic field. It is known that chemical reaction constants, responsible for the potential chemical heat defect, could be affected by the magnetic field. For the chemical reactions responsible for the chemical heat defect in water calorimeters this data is lacking, therefore for the described water calorimeter, the chemical heat defect at 1.5 T is considered zero. LET and dose-rate are known to influence the chemical heat defect. However, these have not fundamentally changed for the MRI-linac used in this study.

Therefore, it is assumed that also in the presence of a magnetic field, a zero-chemical heat defect is valid within the relative standard uncertainty of 0.2%.

An indirect comparison of this study's D_w results with alanine dosimeters operated in an MRI-linac traceable to the NPL primary absorbed dose standard operated at 0 T showed excellent agreement of better than 0.3% (Billas *et al* 2018). Here, the degrees of equivalence of NPL and VSL were taken into account (Allisy *et al* 2009). These results indicate that no significant effects in calorimetric D_w measurement were overlooked. However, they do not rule them out either, including changes in the calorimeter heat defect for which future investigation is needed.

The potential temperature effect due to the magneto-caloric effect (MCE) $\Delta T_{w,ad,MCE}$ is expected to be -0.06 μK. Variation of magnetic field during calorimetric measurement might lead to erroneous results due to this effect.

Calorimeter temperature was recorded during the MRI magnet ramp-down. No change in water temperature was detected beyond the uncertainty of 0.20 mK. It is noted that a $\Delta T_{w,ad,MCE}$ of -0.06 μK would not have been detectable. As a change in c_p with magnetic field would lead to a sudden change in water temperature, it was concluded that it is adequate to apply the same c_p for 0 T and 1.5 T.

D_w measurements with the high-purity cell (HPC) were performed parallel to and perpendicular to a 1.5 T magnetic field as well as at 0 T. These measurements were normalized to the external transmission monitor positioned at the top of the bore. A previous experiment showed that an additional uncertainty of 0.16% needed to be applied when normalizing the calorimetric D_w measurement to the applied monitor system in order to compare D_w measurements performed on one day to measurements on a different day. Furthermore, ratios between D_w measurement obtained at 0 T and 1.5 T with a rotated HPC were comparable and therefore the effect of HPC orientation in the magnetic field was considered insignificant. This confirms the validity of measured radiation induced temperature change, ΔT_w, and the calorimeter correction factors k_C and k_{HPC}, determined for both orientations.

This study confirms that the uncertainty contributions in determination of absorbed dose to water, D_w, with the VSL water calorimeter in a 1.5 T, compared to 0 T, are negligible. Therefore, the uncertainty for calorimetric absorbed dose measurements on-site in an MRI-linac is the same as reported earlier (de Prez *et al* 2016a, 2018) where it was estimated to be 0.37% ($k = 1$). However, due to the applied monitor system in the current study, an additional 0.16% ($k = 1$) is included for day-to-day variations when measured D_w are normalized for MRI-linac output. This uncertainty needs to be applied when comparing results measured on different days and thus also when the calorimeter is used for ion chamber calibrations. Recent improvements in the linac internal monitor system would probably eliminate this uncertainty in future measurements.

The water calorimeter described in this study is currently the only primary standard available for measurement in a magnetic field. This study showed that no additional corrections are needed for operation in a magnetic field. Established methods applied at 0 T can be used in a magnetic field with additional care for geometric alignment. The calorimeter performance is therefore considered to be independent of magnetic field, including orientation and direction of both field and radiation beam, with an uncertainty of 0.37% ($k = 1$).

5. Conclusion

This study successfully characterized and commissioned a water calorimeter as a primary standard of absorbed dose to water with an uncertainty of 0.37% ($k = 1$). All parameters in the determination of the absorbed dose to water were either independent on the magnetic field or can be determined in the presence of a magnetic field. Developments in radiotherapy continue rapidly and the radiotherapy community cannot be delayed until such traceability framework is established. The VSL calorimeter is currently the only primary standard that provides direct access to international traceability framework for absorbed dose to water in the presence of a magnetic field.

Acknowledgments

This project has received funding from the EMPIR programme, grant 15HLT08 'Metrology for MR guided Radiotherapy', co-financed by the Participating States and from the European Union's Horizon 2020 research and innovation programme. I am grateful for discussions with Dr Andrea Peruzzi and Rien Bosma, colleagues at the VSL Contact Thermometry department.

ORCID iDs

Leon de Prez https://orcid.org/0000-0002-7470-4356
Jacco de Pooter https://orcid.org/0000-0002-7542-257X

References

Aalbers A H L, Hoornaert M-T, Minken A, Palmans H, Pieksma M W H, de Prez L A, Reynaert N, Vynckier S and Wittkämper F W 2008 NCS report 18: code of practice for the absorbed dose determination in high energy photon and electron beams Report 18 (The Netherlands: Nederlandse Commissie voor Stralingsdosimetrie Delft)

Allisy P J, Burns D T and Andreo P 2009 International framework of traceability for radiation dosimetry quantities *Metrologia* **46** S1–8

Andreo P, Burns D, Hohlfield K, Huq M S, Kanai T, Laitano F, Smyth V G and Vynckier S 2006 Absorbed dose determination in external beam radiotherapy: an international code of practice for dosimetry based on absorbed dose to water *Technical Report Series* 398 (Vienna: International Atomic Energy Agency)

Andreo P, Burns D, Nahum A, Seuntjens J and Attix F H 2017 *Fundamentals of Ionizing Radiation Dosimetry* (New York: Wiley)

Billas I, de Prez L, de Pooter J and Duane S 2018 Reference dosimetry in MRI-linac using alanine detector *6th MR in RT Symp. (Utrecht)*

Büermann L, Guerra A S, Pimpinella M, Pinto M, Pooter J D, de Prez L, Jansen B, Denoziere M and Rapp B 2016 First international comparison of primary absorbed dose to water standards in the medium-energy x-ray range *Metrologia* **53** 06007

de Prez L A, de Pooter J A, Jansen B J, Aalbers T and Aalbers A H L 2016a A water calorimeter for on-site absorbed dose to water calibrations in ^{60}Co and MV-photon beams including MRI incorporated treatment equipment *Phys. Med. Biol.* **61** 5051–76

de Prez L, de Pooter J, Jansen B, Perik T and Wittkämper F 2018 Comparison of k_Q factors measured with a water calorimeter in flattening filter free (FFF) and conventional flattening filter (cFF) photon beams *Phys. Med. Biol.* **63** 045023

de Prez L, de Pooter J, Jansen B, Wolthaus J, van Asselen B, Woodings S, Soest T, Kok J and Raaymakers B 2016b TH-CD-BRA-05: first water calorimetric D_w measurement and direct measurement of magnetic field correction factors, KQ,B, in a 1.5 T B-field of an MRI linac *Med. Phys.* **43** 3874

Domen S R 1982 An absorbed dose water calorimeter: theory, design, and performance *J. Res. Natl Bur. Stand.* **87** 211–35

Fallone B G 2014 The rotating biplanar linac-magnetic resonance imaging system *Semin. Radiat. Oncol.* **24** 200–2

Franco V, Blázquez J S, Ipus J J, Law J Y, Moreno-Ramírez L M and Conde A 2018 Magnetocaloric effect: from materials research to refrigeration devices *Prog. Mater. Sci.* **93** 112–232

IAPWS 2014 International Association for the Properties of Water and Steam Moscow *Revised Release on the IAPWS Formulation 1995 for the Thermodynamic Properties of Ordinary Water Substance for General and Scientific Use (Revised Release 2014)* ed T Petrova and R B Dooley (Moscow: International Association for the Properties of Water and Steam)

Keall P J, Barton M and Crozier S 2014 The Australian magnetic resonance imaging-linac program *Semin. Radiat. Oncol.* **24** 203–6

Kessler C, Burns D, Jansen B J, de Pooter J A and de Prez L A 2018 Comparison of the standards for absorbed dose to water of the VSL, The Netherlands, and the BIPM for ^{60}Co γ rays *Metrologia* **55** 06012

Klassen N V and Ross C K 1997 Water calorimetry: the heat defect *J. Res. Natl Inst. Stand. Technol.* **102** 63–74

Krauss A 2006 The PTB water calorimeter for the absolute determination of absorbed dose to water in ^{60}Co radiation *Metrologia* **43** 259–72

Krauss A and Kramer H-M 2003 The heat defect in the PTB water calorimeter: a discussion on uncertainty *Workshop on Recent Advances in Absorbd Dose Standards* ed R Huntley *et al* (Melbourne: ARPANSA) pp 15–6

Lagendijk J J W, Raaymakers B W and van Vulpen M 2014 The magnetic resonance imaging-linac system *Semin. Radiat. Oncol.* **24** 207–9

McEwen M, DeWerd L, Ibbott G, Followill D, Rogers D W O, Seltzer S and Seuntjens J 2014 Addendum to the AAPM's TG-51 protocol for clinical reference dosimetry of high-energy photon beams *Med. Phys.* **41** 041501

Meijsing I, Raaymakers B W, Raaijmakers A J E, Kok J G M, Hogeweg L, Liu B and Lagendijk J J W 2009 Dosimetry for the MRI accelerator: the impact of a magnetic field on the response of a Farmer NE2571 ionization chamber *Phys. Med. Biol.* **54** 2993–3002

Mutic S and Dempsey J F 2014 The ViewRay system: magnetic resonance-guided and controlled radiotherapy *Semin. Radiat. Oncol.* **24** 196–9

O'Brien D J and Sawakuchi G O 2017 Monte Carlo study of the chamber-phantom air gap effect in a magnetic field *Med. Phys.* **44** 3830–8

Oborn B M, Metcalfe P E, Butson M J and Rosenfeld A B 2010 Monte Carlo characterization of skin doses in 6 MV transverse field MRI-linac systems: effect of field size, surface orientation, magnetic field strength, and exit bolus *Med. Phys.* **37** 5208–17

OIML 2007 VOCABULARY OIML V 2-200 edition 2007 (E/F) *Int. Vocabulary of Metrology—Basic and General Concepts and Associated Terms (Paris)* (VIM)

Overweg J, Raaymakers B, Lagendijk J and Brown K 2009 System for MRI guided radiotherapy *Proc. Int. Soc. Mag. Reson. Med.* **17** 594

Palmans H 2000 *Proc. of NPL Workshop on Recent Advances in Calorimetric Absorbed Dose Standards* Experimental verification of simulated excess heat effects in the sealed water calorimeter

Picard S, Burns D T, Roger P, de Prez L A, Jansen B J and Pooter J A 2017 Key comparison BIPM.RI(I)-K6 of the standards for absorbed dose to water of the VSL, Netherlands and the BIPM in accelerator photon beams *Metrologia* **54** 06005

Raaijmakers A J E, Raaymakers B W and Lagendijk J J W 2008 Magnetic-field-induced dose effects in MR-guided radiotherapy systems: dependence on the magnetic field strength *Phys. Med. Biol.* **53** 909–23

Raaymakers B W *et al* 2009 Integrating a 1.5 T MRI scanner with a 6 MV accelerator: proof of concept *Phys. Med. Biol.* **54** N229–37

Raaymakers B W, Raaijmakers A J E, Kotte A N T J, Jette D and Lagendijk J J W 2004 Integrating a MRI scanner with a 6 MV radiotherapy accelerator: dose deposition in a transverse magnetic field *Phys. Med. Biol.* **49** 4109–18

Reynolds M, Fallone B G and Rathee S 2013 Dose response of selected ion chambers in applied homogeneous transverse and longitudinal magnetic fields *Med. Phys.* **40** 042102

Rumble J R, Lide D R and Bruno T J 2018 *CRC Handbook of Chemistry and Physics* 99th edn (Boca Raton, FL: CRC Press)

Seltzer S M, Bartlett D T, Burns D T, Dietze G, Menzel H-G, Paretzke H G and Wambersie A 2011 ICRU report 85 fundamental quantities and units for ionizing radiation *Radiat. Prot. Dosim.* **150** 550–2

Seuntjens J and Duane S 2009 Photon absorbed dose standards *Metrologia* **46** S39–58

Seuntjens J and Palmans H 1999 Correction factors and performance of a 4 °C sealed water calorimeter *Phys. Med. Biol.* **44** 627–46

Smit K, van Asselen B, Kok J G M, Aalbers A H L, Lagendijk J J W and Raaymakers B W 2013 Towards reference dosimetry for the MR-linac: magnetic field correction of the ionization chamber reading *Phys. Med. Biol.* **58** 5945–57

Szymanowski H, Baek W Y, Neungang-Nganwa R, Nettelbeck H and Rabus H 2015 PO-0850: MRI-linac: effect of the magnetic field on the interaction cross sections *Radiother. Oncol.* **115** S431

van Asselen B, Woodings S J, Hackett S L, van Soest T L, Kok J G M, Raaymakers B W and Wolthaus J W H 2018 A formalism for reference dosimetry in photon beams in the presence of a magnetic field *Phys. Med. Biol.* **63** 125008

Woodings S J *et al* 2018 Beam characterisation of the 1.5 T MRI-linac *Phys. Med. Biol.* **63** 085015